

GT2017-63204

## INVESTIGATION OF LEAN COMBUSTION STABILITY, PRESSURE DROP, AND MATERIAL DURABILITY IN POROUS MEDIA BURNERS

**Sadaf Sobhani \***

Department of Mechanical Engineering  
Stanford University  
Stanford, California 94305  
Email: ssobhani@stanford.edu

**Bret Haley**

**Dave Bartz**

Alzeta Corporation  
Santa Clara, California 95054

**Jared Dunnmon**

Department of Mechanical Engineering  
Stanford University  
Stanford, California 94305

**John Sullivan**

Alzeta Corporation  
Santa Clara, California 95054

**Matthias Ihme**

Department of Mechanical Engineering  
Stanford University  
Stanford, California 94305

### ABSTRACT

The operational stability and thermal durability of combustion in two-zone porous media burners (PMBs) is examined experimentally and computationally. Long-term material durability tests at constant and cycled on-off conditions are performed, along with a characterization of combustion stability, pressure drop and pollutant emissions for a range of equivalence ratios, mass flow rates, and burner setups. Experimental thermocouple temperature measurements and pressure drop data are presented and compared to results obtained from one-dimensional volume-averaged simulations. Experimental and model results show good agreement for temperature profiles and pressure drop evaluated using the Darcy-Forchheimer equation with Ergun's relations. Enhanced flame stability is observed for burners with Yttria-stabilized Zirconia Alumina (YZA) upstream and Silicon Carbide (SiC) in the downstream combustion zone. Measurements of product gas concentrations illustrate highest emissions of CO at conditions close to flash-back and, as expected, higher NO<sub>x</sub> emissions with increasing equivalence ratios.

### NOMENCLATURE

$D_{ij}$	Species i binary diffusion coefficient (m/s)
$MFR$	Mass flux rate (kg/m <sup>2</sup> s)
$Pe$	Peclet number ( $Pe = \frac{SLd_{p,eff}\rho_g c_g}{\lambda_g}$ )
$S_L$	Laminar flame speed (m/s)
$X_i$	Species i mole fraction
$Y_i$	Species i mass fraction
$c$	Specific heat capacity (J/kgK)
$d_p$	Pore diameter (m)
$h_v$	Volumetric heat transfer coefficient (W/m <sup>3</sup> K)
$\dot{m}$	Mass flow rate (kg/s)
$\dot{q}$	Heat release rate (W/m <sup>3</sup> )
$u$	Volume-averaged fluid velocity (m/s)
$\varepsilon$	Porosity
$\lambda$	Thermal conductivity (W/mK)
$\kappa$	Radiative heat extinction coefficient (W/m <sup>2</sup> K)
$\Omega$	Scattering albedo
$\dot{\omega}_i$	Species i production rate per unit volume (kg/m <sup>3</sup> s)
$\phi$	Equivalence ratio
$\rho$	Density (kg/m <sup>3</sup> )
$\sigma$	Stefan-Boltzmann constant (W/m <sup>2</sup> K <sup>4</sup> )

\*Address all correspondence to this author.

$g$	Gas phase subscript
$s$	Solid phase subscript
$eff$	Effective property in the porous matrix subscript

## INTRODUCTION

As emission regulations become increasingly more stringent and policies evolve to combat global climate change impacts, reducing pollutant and greenhouse gas emissions emerge as one of the most important goals of combustion research. Techniques such as staged combustion, catalytic combustion, and advanced mixing and fuel atomization are some of the methods developed to reduce emissions of pollutants such as nitrogen oxides ( $NO_x$ ), carbon monoxide (CO), and unburned hydrocarbons (UHCs) [1, 2]. The implementations of advanced combustion concepts, such as porous media combustion, represent other techniques that are capable of achieving low emissions, enhanced flame stabilization, and improved fuel efficiency.

Combustion of a gas mixture within the cavities of an inert porous medium exhibits characteristics different from those of conventional burners that utilize a free flame. Specifically, porous media burners (PMBs) operate on the principle that the solid porous matrix serves as a means of internally recirculating heat from the combustion products upstream to the reactants, termed “excess enthalpy combustion” [3]. Heat transferred from the flame to the solid is circulated both via solid conduction and long range solid-to-solid radiation, and transferred to the unburned gas mixture by convection. The large solid-gas interfacial surface area of PMBs facilitates effective heat transfer between the two phases. The higher temperatures of the preheated reactants lead to a faster flame speed and enhanced power output, while the gas-to-solid convection downstream of the flame decreases the gas temperature in the reaction zone and the exhaust gas, thereby reducing the formation of thermal  $NO_x$  [4, 5]. Porous media refers to any materials with connected voids that facilitate fluid flow. The geometries considered in numerical and experimental investigations of PMBs include packed beds of spheres, arrays of staggered cylinders, fiber lamellae, and ceramic or metal foams.

The internal recirculation of heat in PMBs has several implications on the flammability limit of the fuel-air mixture. The lean flammability limit of a fuel-air mixture decreases as the initial temperature of the mixture increases, and therefore excess enthalpy-burning can lead to a reduction in this lower limit [6]. The practical advantages of extending the lean flammability limit include lower emissions, reduced thermal stresses due to decreased flame temperatures, and complete fuel conversion due to lean combustion. However, the challenge lies in stabilizing these flames inside the porous matrix in the presence of complex thermophysical, transport, and heat-transfer processes. The energy released during chemical reactions is coupled with the conjugate heat transfer inside the porous structure, which results from

strong heat exchange in the reaction zone. Although a detailed understanding of the underlying processes at the pore-scale is largely incomplete at the current state [7], both experimental and numerical studies have demonstrated advantages in flame stability, pollutant emissions, and lean flammability in PMBs both at atmospheric conditions and elevated pressures [8–14].

The modified Peclet number characterizes the local ratio of heat release by combustion to heat removal in a PMB [15]. Flame stability is observed at the interface between the two regions of high and low pore-density, corresponding to regions above and below the critical Peclet number for flame quenching. Most existing PMBs utilize this critical dimensionless number in an “interface-stabilized” burner design, which operates on the principle that the upstream region serves as a flame-arrestor. This implies that a material with low thermal conductivity, allowing only for a limited amount of heat transport upstream, would be beneficial in the upstream region to prohibit flame propagation against the flow direction. Barra et al. [16] performed numerical simulations to examine the effects of the properties of the flame-arrestor section at lean conditions and found that, in fact, solids with low thermal conductivity and convective heat transfer coefficients are predicted to have the largest stable operating range.

The objective of this study is to experimentally examine the effect of material, geometric and thermal properties on flame stability and determine the limits for flame blow-off and flash-back in an “interface-stabilized” burner. Additionally, this study aims to determine the accuracy of volume-averaged models for predicting the temperature distribution and pressure drop in PMBs. To accomplish these objectives, two materials of different thermal conductivities, namely Yttria-stabilized Zirconia Alumina (YZA) and Silicon Carbide (SiC), are tested in five different configurations and across a range of equivalence ratios and mass flow rates to identify trends in flame stability behavior. The temperature predictions of a 1D volume-averaged model with detailed chemistry are assessed against thermocouple measurements from the burner. Pressure drop is computed with the Darcy-Forchheimer equation [17], using Ergun’s relations for the drag and permeability coefficients [18], and compared to experimental measurements. Since these models for pressure drop were developed for non-reacting flows in unconsolidated porous media, a representative length scale comparable to the particle diameter in consolidated reticulated foams is required to compute the pressure drop. Three different length scales are considered and compared with experimental measurements. Furthermore, for the burner design with optimal pressure drop and stability properties, durability studies were performed for over 400 hours of continuous testing and 1229 cycle tests. Life-cycle durability analysis of these materials along with trends in pollutant formation and flame stability help further the optimization of existing PMB technology with potential applications to propulsion, stationary gas turbines, waste-heat recovery, reformers, and domes-

tic heating units.

## EXPERIMENTAL APPARATUS AND PROCEDURE

The burner tested in this study employs a two-zone “interface-stabilized” burner concept, which consists of an upstream matrix with high pore-density that acts as a flame arrestor and a downstream porous section with lower pore-density in which combustion is facilitated. Figure 1 illustrates the setup, with the top-most porous sample referred to as the downstream section and the bottom two samples acting as the upstream flame-arrestor. Pore-density is measured in pores per inch (ppi) and the porosity,  $\epsilon$ , refers to the fraction of void volume to the total volume.

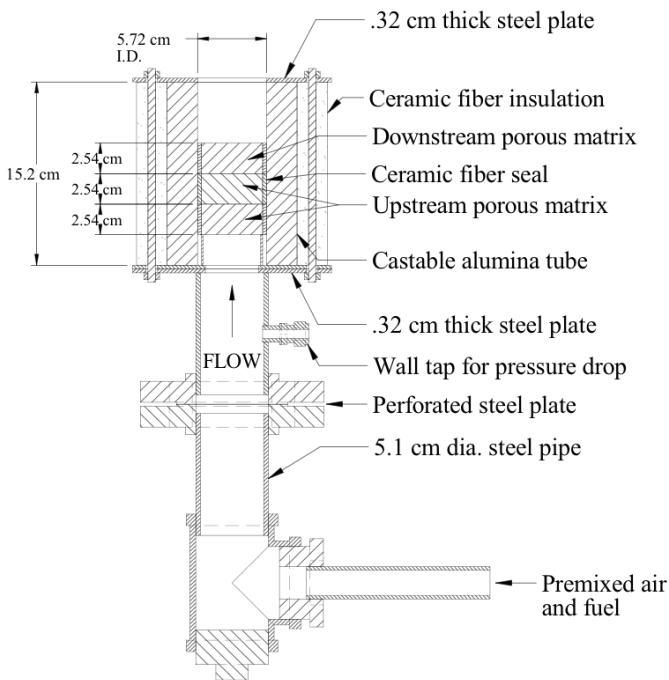


**FIGURE 1:** CROSS-SECTIONAL SCHEMATIC OF EXPERIMENTAL APPARATUS.

The present study utilizes ceramic reticulated foams due to their high porosities and consequently low pressure drops. The ceramic reticulated foams used in the upstream and downstream sections of the PMB are varied in the experimental investigation. The pore diameter in the upstream section corresponds to a Peclet number below  $65 \pm 45$ , and conversely for the downstream

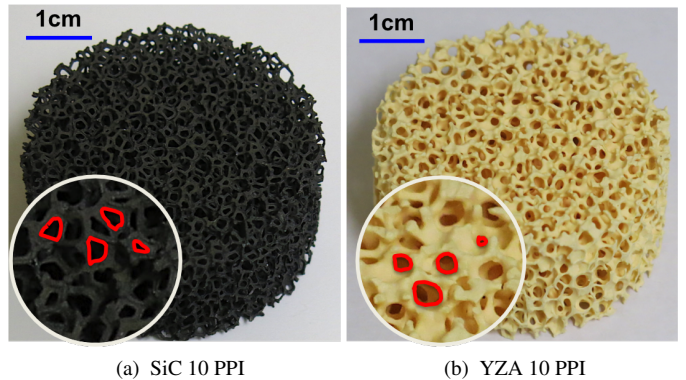


**FIGURE 2:** CERAMIC RETICULATED FOAM SAMPLES USED IN THIS STUDY, WITH A FEW PORES OUTLINED TO ILLUSTRATE THE DIFFERENCE IN PORE GEOMETRY.

section [19]. Samples of SiC and YZA were used in five different arrangements, as summarized in Table 1. The reticulated SiC foams (Ultramet, Pacoima, CA) are made using chemical vapor deposition (CVD) of SiC, which coats the ligaments of the underlying non-crystalline vitreous carbon foam structure. The YZA foams (Selee Corporation, Hendersonville, NC), similar to the underlying carbon foam of the SiC, are made via the sponge replication process and are composed of 62% zirconia, 33% alumina, 2% yttria and 3% calcia. Figure 2 shows the relative similarity between the two structure topologies and also illustrates the difference between the circular pores of the YZA and the polygonal pores of the SiC. Furthermore, from inspection, the presence of closed pores in the YZA sample is evident, which can affect the pressure drop and flow behavior. For the five different pore densities used, ranging from 3 to 65 ppi, the porosity of the samples varies linearly between 91% to 83%, respectively.

The porous media specimen were stacked in a castable alumina tube (Western Industrial Ceramics, Santa Fe Springs, CA) and wrapped in ceramic paper (Unifrax, Tonawanda, NY) for sealing and insulation.

The experiments were performed using natural gas, composed of about 95% methane, 4% ethane, 1% carbon dioxide and <1% of other hydrocarbons, based on molar concentration. Upstream, the fuel and air streams are properly mixed by first converging within a tee-fitting, then flowing through a length equal to 63 pipe diameters, including four 90° elbows, before entering the apparatus (Fig. 1). Premixed air and natural gas are supplied to the burner and ignited at the 0.32 cm steel plate downstream of the porous media. The flow conditions for stable operation of the reaction are subsequently investigated. The occurrence of flame instability in PMBs is challenging to identify experimentally since it is a gradual process, unlike a free flame that extinguishes immediately after the system reaches an imbalance

Burner	Upstream Flame-Arrestor (material, ppi)	Downstream Combustion Section (material, ppi)
1	SiC, 65	SiC, 10
2	YZA, 60	SiC, 10
3	YZA, 40	SiC, 10
4	YZA, 40	YZA, 10
5	YZA, 40	SiC, 3

**TABLE 1:** SPECIFICATIONS OF CONFIGURATIONS AND PORE DENSITY (PPI) OF THE FIVE BURNERS. BURNERS WERE COMPOSED OF TWO POROUS SAMPLES IN THE UPSTREAM SECTIONS AND ONE IN THE DOWNSTREAM SECTIONS; EACH SAMPLE HAS A HEIGHT OF 2.54 CM.

with the flame speed. In this study, stable operation is identified as a stationary flame within the downstream combustion section, determined by measuring the temperature along the flow axis. Flashback was recorded if the temperature detected by the thermocouple upstream of the interface surpassed 755K (Fig. 3). Blow-off occurred in two stages. During the first stage of blow-off, the flame departs from the interface between the upstream and downstream sections, which is detected by a sharp decrease in temperature near the interface. This behavior is followed by partial or total departure of the flame-front from the downstream section, which is detected visually. For stability tests, adjustments in the mass flux and equivalence ratio were made until the flame indicated either flash-back or blow-off. To check repeatability, the high mass-flux limit (i.e. blow-off) was repeated at least 3 times, and the low mass-flux limit (i.e. flash-back) was repeated at least 2 times for each equivalence ratio value. Within each series, blow-off or flash-back generally occurred at the same circumferential position, and variations in mass-flux at the point of instability were generally within 5-10%.

To measure the flow rate, five rotameters were utilized; two for natural gas, and three for air. Rotameters with the smallest maximum flow rate that fit the test series were used for each experiment. Two differential pressure gauges were used; the first measured the combustion air pressure at the rotameter exits, the second measured the pressure drop across the PMB (Dwyer Magnehelic, Michigan City, IN).

The burner was instrumented with thermocouples, with a 90° separation azimuthally and 0.635 cm separation axially (Fig. 3). Two thermocouples were placed at each axial location with a 180° separation, but they slightly shifted axially during the experiment and their updated locations are reflected in the results (labeled A–D in Fig. 6). All thermocouples were mineral-

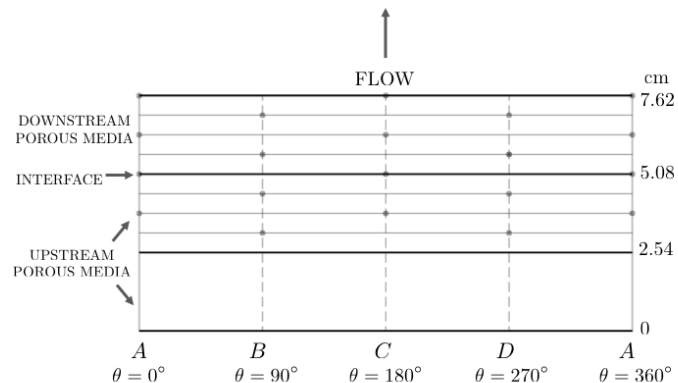


**FIGURE 3:** LOCATION OF THE THERMOCOUPLES, REFERRED TO AS A-D, AT THE BURNER OUTER DIAMETER.

insulated type-K units with standard limits (Watlow Gordon, Richmond, IL). Since only lean mixtures were tested in this experiment, thermocouples with higher temperature tolerances were not required. Grounded junction thermocouples measured axial temperatures and exposed junction thermocouples measured exhaust temperatures. All temperature data was captured with three Pico Technology TC-08 thermocouple data loggers.

Emissions were sampled with an ECOM EN2-F Portable Emissions Analyzer. The measured species, range, accuracy and resolution are as follows: O<sub>2</sub>, 0-21% by volume, ± 0.2%, 0.1%; CO, 0-10,000 parts per million (ppm), ± 2%, 1 ppm; NO, 0-5000 ppm, ± 5%, 0.1 ppm; NO<sub>2</sub>, 0-100 ppm, ± 5%, 0.1 ppm. An Ametek Thermoxy CMFA-P Portable Premix Analyzer (accuracy is the greater of ± 2% of measured and ± 0.1% O<sub>2</sub>) was used to measure the O<sub>2</sub>-content.

## NUMERICAL MODEL

A computational study was conducted to compare model predictions for pressure drop and temperature against the experimental measurements. The computational model was developed using a volume-averaged two-zone formulation [20]. The equations governing the combustion of the gaseous fuel in porous media are continuity, energy, and species conservation (Eqs. 1). To account for the energy transfer between the solid and gas phases, two separate energy equations are solved for both media (Eq. 1c & 1d). The effects of conduction and radiation in the solid phase, and heat exchange between solid and gas are incorporated in the equations. Dufour and Soret effects are neglected; momentum conservation is also not included. In this model, we assume that (i) the solid is inert and does not react with the gas mixture, (ii) there is thermal non-equilibrium between the gas and the solid matrix (two-medium model), (iii) the heat transfer between the

two phases is proportional to their temperature difference, (iv) the solid can be modeled as gray body, and (v) gaseous radiation is negligible. The resulting equations take the following form [16, 20, 21]:

$$\partial_t(\rho_g \varepsilon) + \partial_x(\varepsilon \rho_g u) = 0, \quad (1a)$$

$$\varepsilon \rho_g (\partial_t Y_i + u \partial_x Y_i) = -\partial_x(\varepsilon \rho_g V_i Y_i) + \varepsilon \dot{\omega}_i, \quad (1b)$$

$$\varepsilon \rho_g c_g (\partial_t T_g + u \partial_x T_g) = \partial_x(\lambda_g \partial_x(\varepsilon T_g)) \quad (1c)$$

$$-\rho_g \left( \sum_{i=1}^{N_s} c_{g,i} V_i Y_i \right) \partial_x(\varepsilon T_g) \\ - h_v(T_g - T_s) + \varepsilon \dot{q}, \quad (1d)$$

$$\rho_s c_s \partial_t((1-\varepsilon)T_s) = -\partial_x(\lambda_{s,eff} \partial_x T_s) - \partial_x \dot{q}_R + h_v(T_g - T_s)$$

The diffusion velocity of species  $i$  is written as:

$$V_i = -D_{im} \partial_x \ln(X_i), \quad (2)$$

where the species mixture diffusivities are evaluated using the Hirschfelder-Curtiss approximation [22]:

$$D_{im} = \frac{1 - Y_i}{\sum_{\substack{i=1 \\ i \neq j}}^{N_s} X_j / D_{ij}}. \quad (3)$$

The radiative source term, appearing in Eq. (1d) takes the form:

$$\partial_x \dot{q}_R = 2\kappa(1-\Omega) (2\sigma T_s^4 - [\dot{q}_R^+ + \dot{q}_R^-]), \quad (4)$$

where the radiant heat fluxes in forward and backward direction are expressed as:

$$d_x \dot{q}_R^+ = -\kappa(2-\Omega) q_R^+ + \kappa\Omega q_R^- + 2\kappa(1-\Omega)\sigma T_s^4, \quad (5a)$$

$$-d_x \dot{q}_R^- = -\kappa(2-\Omega) q_R^- + \kappa\Omega q_R^+ + 2\kappa(1-\Omega)\sigma T_s^4. \quad (5b)$$

The gas and solid energy equations are coupled by the convective heat transfer,  $h_v(T_g - T_s)$ , where  $h_v$  for ceramic foams is used [23]. The effective thermal conductivity in the porous solid is estimated from manufacturer data. The Discrete-Ordinates two-flux method was used to model the radiant source term in the solid phase energy equation (Eq. 5) [24]. The radiative heat extinction coefficient,  $\kappa$ , is based on a geometric optics model that was validated by Hsu and Howell [25], evaluated as  $\kappa = 3(1-\varepsilon)/d_p$ . The boundary conditions for solving Eqs. 1 are given in Table 2. Combustion simulations were performed using the CANTERA [26] one-dimensional reacting flow solver, which was adapted to account for the coupling between the gas and solid phases.

## Pressure Drop

The pressure drop was evaluated using the Darcy-Forchheimer equation:

$$d_x P = -\frac{\mu}{K_1} u - \frac{\rho}{K_2} u^2, \quad (6)$$

where  $K_1$  is the intrinsic permeability and  $K_2$  is the non-Darcian drag coefficient, estimated using Ergun's equation [18]:

$$K_1 = \frac{d^2 \varepsilon^3}{150(1-\varepsilon)^2}, \quad (7a)$$

$$K_2 = \frac{d \varepsilon^3}{1.75(1-\varepsilon)}. \quad (7b)$$

Ergun's empirical relations were developed for unconsolidated media made of solid spherical particles, therefore  $d$  in Eq. (7) refers to the particle diameter. These relations, along with most models used for the prediction of permeability parameters of ceramic foams, are based on the particle diameter as the characteristic length scale. The major difficulty in applying these models to porous foams is in defining representative structural properties of a foam to replace the particle diameter in Ergun's model. Philipse et al. [17] first illustrated that Ergun-type permeability models based on granular media also apply to foams, simply by replacing the particle diameter with the pore diameter, extracted from image analysis, as the characteristic length. Several other attempts have been presented in the literature to replace the particle size in Ergun's relations. Innocentini et al. [27] used the cylindrical form of the hydraulic diameter ( $d_h = 1.5 \frac{1-\varepsilon}{\varepsilon} d$ ) to derive an effective particle diameter from the average pore size of the porous foam,  $d$ . The hydraulic diameter represents the ratio between the volume available for the flow to the total wetted surface. Here, it is assumed that the solid filaments of the porous foam structure are analogous to the particles of a granular media. Dukhan et al. [28] later proposed the reciprocal of the specific surface area ( $d_{SA}$ ) as the equivalent particle diameter, and showed good agreement with experimental measurements for metal foams. This method requires information from the manufacturer about the specific surface area of the foam. Alternatively, optical microscopy or multipoint BET methods can be used to estimate this parameter [28]. Despite the importance and wide-spread use of ceramic foams in several fluid-flow applications, a relationship between their permeability and simple foam structure properties remains uncertain. To address this, the experimental data for pressure drop of this study are compared to the Ergun-type models proposed by [17, 27, 28].

The total pressure drop across the porous matrix is obtained

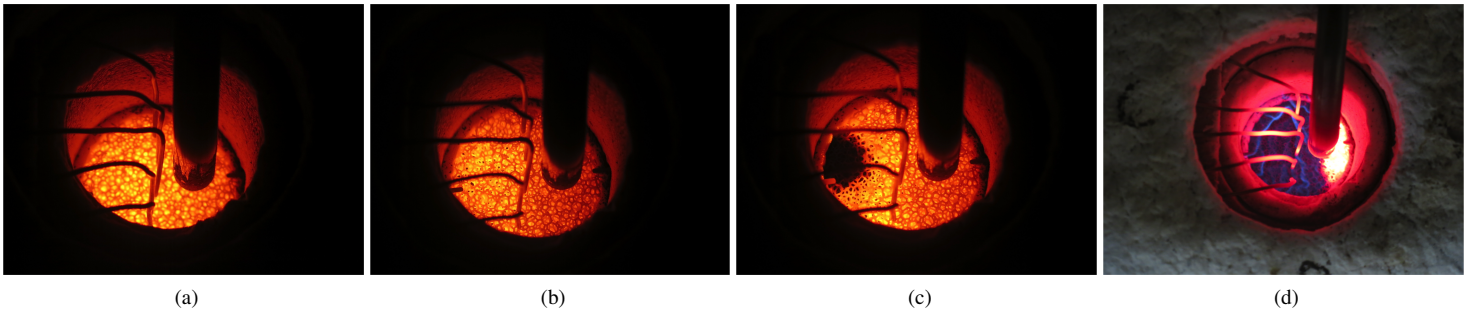


**FIGURE 4:** (a) POROUS MEDIA BURNER DURING STABLE AND (b)-(d) UNSTABLE BLOW-OFF OPERATION. (b) THE FLAME IS APPROACHING THE TOP SURFACE ASYMMETRICALLY. (c) A PORTION OF THE COLD REACTANT MIXTURE HAS REACHED THE TOP SURFACE. (d) THE FLAME HAS REACHED THE TOP SURFACE (I.E. BLOW-OFF). THESE IMAGES FROM ABOVE THE BURNER ILLUSTRATE THE NON-UNIFORMITY IN FLAME BEHAVIOR.

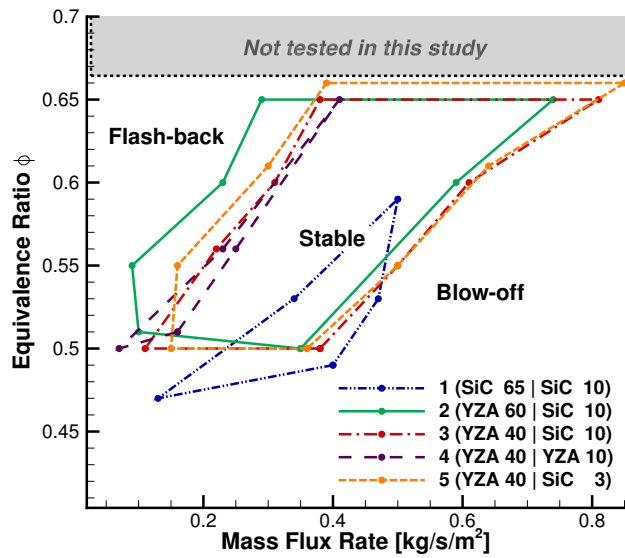


**FIGURE 5:** STABILITY MAP FOR ALL FIVE BURNERS, WITH STABILITY MAXIMIZED FOR BURNER 5.

by integrating Eq. (6) along the axial direction:

$$\Delta P = - \int_0^x \left( \frac{\mu}{K_1 \rho} \frac{\dot{m}}{\varepsilon A} + \frac{1}{K_2 \rho} \left( \frac{\dot{m}}{\varepsilon A} \right)^2 \right) dx, \quad (8)$$

recognizing that the thermoviscous and material properties depend on the spatial location, and using the superficial velocity expressed in terms of the mass flow rate,  $u = \dot{m}/(\varepsilon A \rho)$ .

Inlet conditions	Outlet conditions
$T_g = 300\text{K}$	$d_x T_g = 0$
$d_x T_s = 0$	$d_x T_s = 0$
$Y_i = Y_{i0}$	$d_x Y_i = 0$
$q^+ = \sigma T_s^4$	$q^- = \sigma T_s^4$

**TABLE 2:** BOUNDARY CONDITIONS FOR 1D SIMULATIONS USING VOLUME-AVERAGED MODELS.

In the following, results from these simulations are compared against experimental measurements to assess the accuracy of volume-averaged models applied to porous media combustion.

## RESULTS AND DISCUSSION

### Flame Stability and Temperature Profiles

The five burners tested exhibited varying temperature profiles and stability regimes, associated with the unique thermal and geometric properties of the porous samples comprising the burners. The solid thermal conductivity of YZA foams is 0.30 W/mK and that of the SiC ( $\varepsilon = 0.9$ ) is near 1.5 W/mK (Seleee and Ultramet manufacturer data). With close to five times the thermal conductivity, SiC exhibits favorable flame stability properties when employed in the downstream reaction zone but conversely affects flame stability when employed in the upstream flame-arrestor zone. The small-pore, low-conductivity YZA foam was shown to be a superior upstream flame-arrestor compared to SiC and permitted operation at higher levels of equivalence ratios and mass fluxes.

The higher thermal conductivity of the SiC in the upstream section for burner 1 resulted in flash-back at lower values of

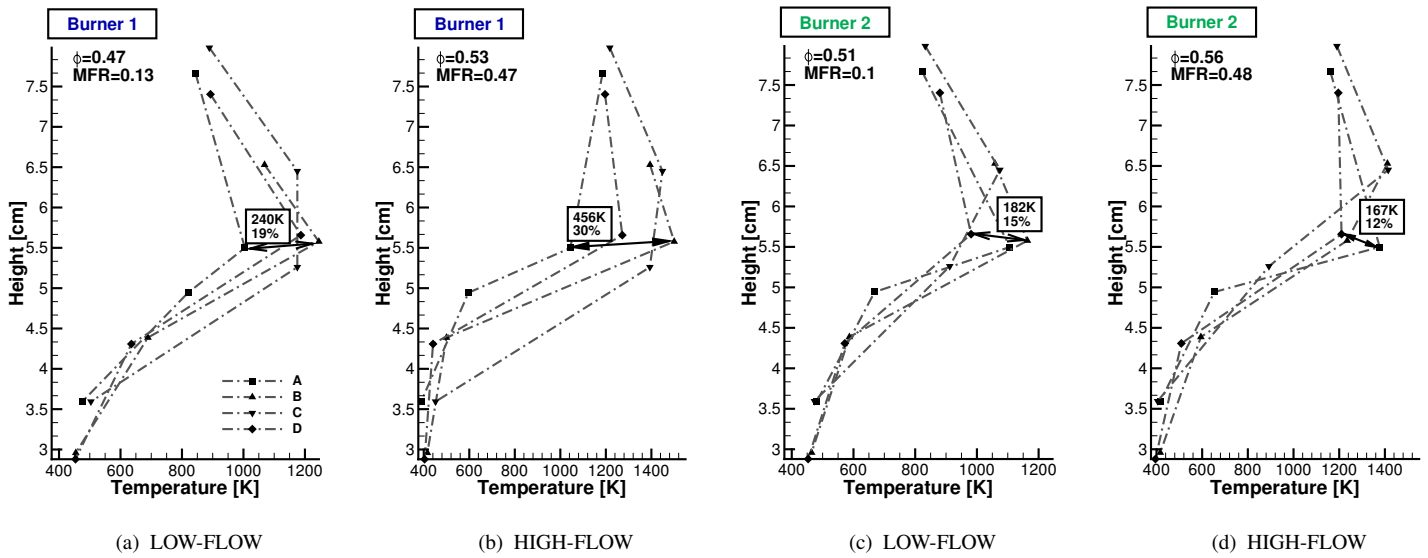


**FIGURE 6:** TEMPERATURE VARIATIONS ALONG AZIMUTHAL DIRECTION BETWEEN THERMOCOUPLES, REFERRED TO AS A-D, AT THE SAME AXIAL LOCATIONS (FIG. 3). MAXIMUM TEMPERATURE VARIATION BETWEEN THERMOCOUPLES LESS THAN 1MM APART ALONG AXIAL DIRECTION IS LABELED ALONG WITH PERCENTAGE DIFFERENT COMPARED TO MAXIMUM TEMPERATURE MEASURED.

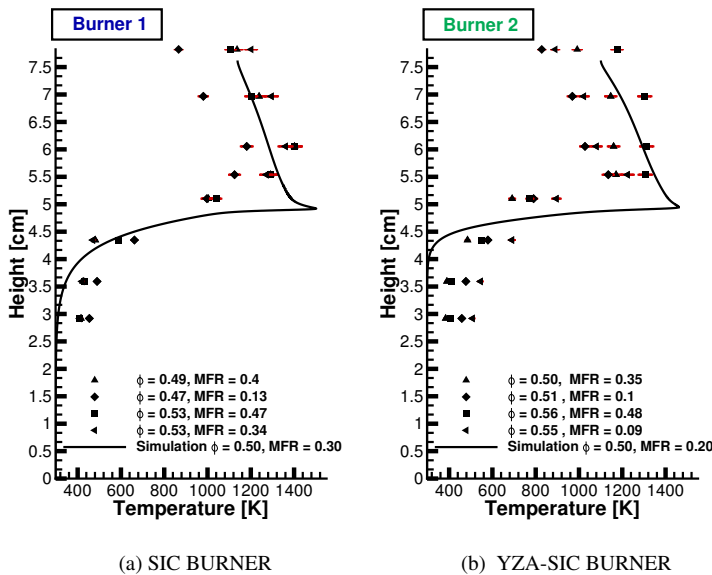


**FIGURE 7:** AVERAGED TEMPERATURE MEASUREMENTS FROM FOUR THERMOCOUPLES COMPARED TO SIMULATION RESULTS FOR BURNER 1 AND 2 AT VARIOUS MASS FLUX RATES (MFR) AND EQUIVALENCE RATIOS  $\phi$ .

equivalence ratio compared to all other burners. Burners 2, 3, and 5 have similar stability performances, with burner 5 achieving the highest mass flux and lowest pressure drop. Burners 1 and 4 had much smaller stability envelopes by comparison. Burner 1, with SiC for both zones of the PMB, was only stable at low mass flux and equivalence ratio test conditions. Burner 4 utilized YZA for both zones of the PMB and blow-off occurred at lower mass flux rates compared to burners 1-3 and 5 (Fig. 5). Figure 4 illustrates the burner blow-off sequence with the flame first embedded in the porous matrix and then approaching the surface. The blow-off initially occurs only on one side of the burner, as evidenced by the cold reactant mixture reaching the top surface. The non-uniformity in the porous media is illustrated by the asymmetric behavior of the flame at blow-off and further confirmed by the temperature variations at each axial location. Azimuthal asymmetries in temperature, as high as 30%, are observed in all five burners and illustrated for burner 1 and 2 in Fig. 6. The source of non-uniformity in temperature and flow behavior is believed to be caused by heterogeneities in porosity and pore distribution or pore-blockage in regions of the foam. Potentially, foams with homogenous structures would enable the ideal uniform temperature distribution and better control of combustion stability.

Figure 7 shows azimuthally averaged temperature measurements from thermocouples at each axial location in comparison to the volume-averaged numerical model. In general, trends in the predicted temperature profiles from the 1D model are in

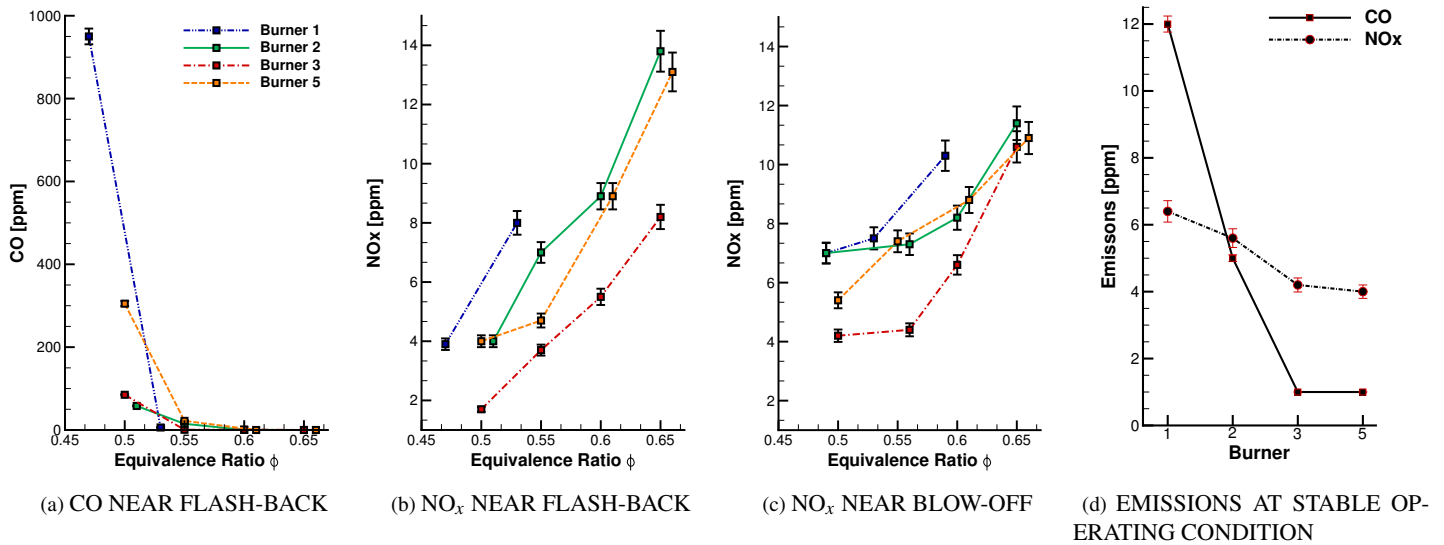


**FIGURE 8:** EMISSIONS FOR BURNERS 1-3 AND 5, CORRECTED TO 3% O<sub>2</sub>. BLOW-OFF, FLASH-BACK, AND STABLE OPERATING CONDITIONS FOR EACH BURNER CORRESPOND TO FIG. 5. (a) CO EMISSIONS NEAR FLASH-BACK CONDITIONS. CO EMISSIONS NEAR BLOW-OFF NOT SHOWN SINCE ALL VALUES ARE NEAR ZERO. (b), (c) NO<sub>x</sub> EMISSIONS NEAR FLASH-BACK AND BLOW-OFF, RESPECTIVELY. (d) NO<sub>x</sub> AND CO AT A COMMONLY STABLE OPERATING CONDITION OF  $\phi=0.5$ , MFR=0.34.

good agreement with averaged experimental temperature measurements. It is important to note that the thermocouple measurements only reveal the local temperature of the pore in which the thermocouple is placed. With only two thermocouples at each axial location, the measurements may not be representative of the temperature distribution. This is especially relevant in the flame-zone where alveolar flames significantly increase local temperatures. Although averaged temperatures from two point measurements are expected to deviate above or below that of the volume-averaged model predictions, the model consistently under-predicts temperatures in the upstream flame-arrestor section, both for the SiC and YZA samples. Dunnmon et al. [7] reported similar trends for a SiC burner operated with methane. In this study, 3D X-ray computed tomography (XCT) measurements were used to interpret the pore-scale temperature field, which was then cross-sectionally averaged and compared to a volume-averaged model. These comparisons also revealed a temperature under-prediction in the upstream section. Non-intrusive, 3D temperature measurements and detailed simulations can help shed light on the pore-scale physics in order to develop enhanced volume-averaged models and effective material parameters. Nonetheless, the model accurately identifies flame location, maximum temperatures, and exit temperatures, which are critical for designing integrated systems where downstream components are temperature sensitive.

### Predictions for High-pressure Conditions

The trends found in flame stability can be extrapolated to high-pressure conditions using the modified Peclet number analysis, which characterizes the ratio of heat release to heat removal in a PMB. Although the critical Peclet number for quenching in porous media can vary, depending on the gas composition and solid matrix temperature [19], a general scaling to elevated pressures can be identified.

$$Pe = \frac{SLd_{p,eff}\rho_g c_g}{\lambda_g} = \frac{SLd_{p,eff}}{\alpha_g}, \quad (9)$$

where  $\alpha_g$  is the gas thermal diffusivity. Laminar flame speed and diffusivity dependence on pressure can be approximated as  $P^{-0.5}$  and  $P^{-1}$ , respectively. Assuming equal temperatures, the following relationship for the effective pore diameter is derived for matching the Pe number at pressure  $P$ :

$$\frac{d_{p,eff}}{d_{o,p,eff}} = \sqrt{\frac{P_o}{P}}, \quad (10)$$

For instance, to match the flame stability properties at an elevated pressure of 10 bar, an upstream porous material with  $\sim \sqrt{10}$  times smaller pores is needed to prevent flash-back. Blow-off

is not a concern since the burning rate increases with increasing pressure and lean blow-out is not dependent upon pressure [14].

## CO and NO<sub>x</sub> Emissions

Figure 8 shows NO<sub>x</sub> and CO emission measurements corrected to 3% O<sub>2</sub> for burners 1-3 and 5, at operating conditions near flash-back, blow-off, and stable flame regimes (Fig. 5). Emissions data for burner 4 are not presented due to poor stability performance, and therefore lack of sufficient data. All emissions are measured 3.2 cm above the top surface of the PMB at the centerline of the burner. At stable operating conditions, emissions of CO and NO<sub>x</sub> were generally low (<15 ppm). Figure 8(d) is an illustrative example of emissions during stable operation. For all conditions, NO<sub>x</sub> emissions increased with increasing equivalence ratios for all burners (Fig. 8(b,c)). This behavior is expected since more heat is released as equivalence ratio increases, enhancing both prompt and thermal NO<sub>x</sub> production pathways. CO emissions were approximately or equal to zero near blow-off conditions, and therefore not shown in Fig 8. Conversely, CO emissions were highest near flash-back conditions, where oxidation rates decrease due to low temperatures (~ 1000K) (Fig. 6). Therefore, incomplete combustion results in higher CO emissions. This phenomena is most pronounced in burner 1, with peak CO emission of 950 ppm. The high thermal conductivity of the SiC in this burner facilitates rapid heat conduction away from the flame zone, potentially hindering CO oxidation. Measurements near the walls of the burner consistently showed higher CO emissions than centerline measurements, which further suggests the role of flame quenching both at the pores and at the walls of the burner. Figure 8(d) illustrates the trend in both CO and NO<sub>x</sub> for burners 1-3 and 5 at a commonly stable operating condition of  $\phi = 0.5$ ,  $MFR = 0.34$ . At this condition, all four burners operate in the regime between flash-back and blow-off, and therefore trends in emissions are attributed to the composition of the burner. The decreasing trend in CO emissions between burner 1 and 2, which are composed of different thermally conductive materials upstream, further illustrates the effect of the upstream section in facilitating reaction zone cooling and impedance of CO oxidation. In addition to the solid matrix heat transport properties, the upstream material pore density also has an effect on emissions. Between burner 2 and burner 3, upstream pore density decreases by 20 ppi, and the result is a decrease in CO emissions. Although the high pore density material in the upstream section of burner 2 extends the limit for flash-back as compared to burner 3 (Fig. 5), the enhanced flame quenching behavior results in higher CO emissions. Consistent with the trends found, stable emissions of burners composed of the same upstream material and pore density, are nearly identical (i.e. burners 3 and 5). Overall, burners with the highest range of stability (i.e. burners 2, 3, 5) exhibit ultra-low emissions characteristics, which is directly relevant to their impact in industrial applications.

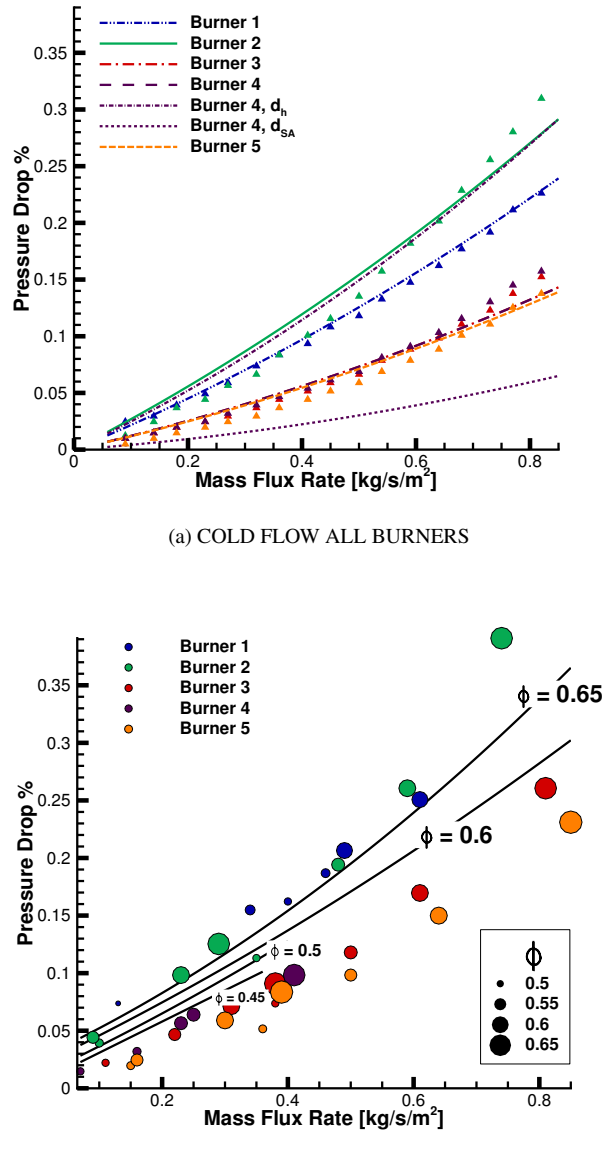


**FIGURE 9:** (a) COMPARISON OF PREDICTED PRESSURE DROP (LINES) AND EXPERIMENTAL RESULTS (SYMBOLS) USING THREE DIFFERENT CHARACTERISTIC LENGTHS FOR BURNER 4 AND THE PORE DIAMETER FROM IMAGE ANALYSIS FOR ALL BURNERS. (b) REACTING FLOW EXPERIMENTAL RESULTS IN THE 5 DIFFERENT BURNERS (CIRCLES), WITH COMPARISON TO COMPUTATIONAL RESULTS (LINES) FOR GEOMETRY AND MATERIALS PROPERTIES MATCHING BURNER 2. DIAMETER OF CIRCLE CORRESPONDS TO EQUIVALENCE RATIO,  $\phi = 0.47 - 0.66$ .

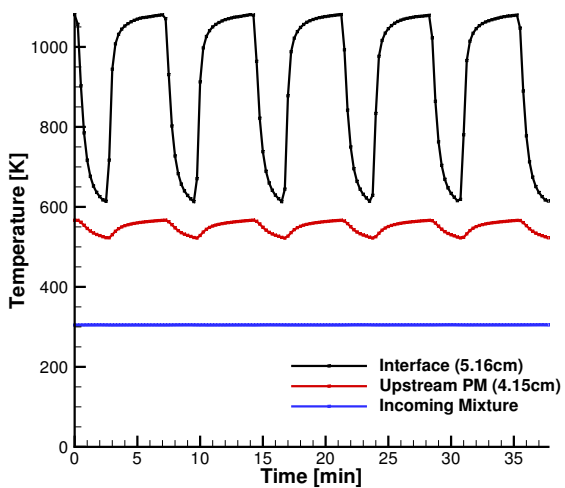


**FIGURE 10:** TEMPERATURE OF PMB DURING CYCLE OPERATION (1229 CYCLES TOTAL), SHOWING 2 MINUTE AIR PURGE, FUEL ADDITION, AND IGNITION. THERMOCOUPLE LOCATIONS ARE WITH RESPECT TO FIG. 3.

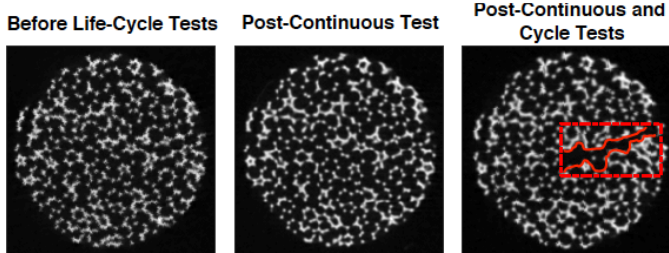


**FIGURE 11:** X-RAY IMAGES SHOWING CRACKING IN THE 3PPI SAMPLE OF BURNER 5.

### Pressure Drop

Pressure drop is analyzed from experimental measurements and simulation predictions. Pressure drop is minimized in burner 5 due to its composition of low pore-density, large pore diameter ceramic foams. For comparison with the Darcy-Forchheimer model, three different commonly used characteristic length scales are evaluated against the experimental data. Results show that computing Ergun's relations using pore diameter  $d$  from image analysis yields better agreement with experimental data, compared to other lengths scales found in the literature (i.e. the hydraulic diameter  $d_h$  and the reciprocal of specific surface area  $d_{SA}$ ). The cold flow pressure drop computed using all three length scales is illustrated in Fig. 9(a) for burner 4, since only the YZA manufacturer provided information about the specific surface area of the foam. Pressure drop calculations using  $d$

from image analysis for all other burners is also shown in this figure. Using the most suitable length scale identified, the predicted pressure drop shows reasonable agreement with the experimental data for both cold and reacting flows (Fig. 9). Results illustrate that all burner designs yield very low pressure drops well below 0.4%.

### Durability Testing

Two durability tests, continuous and cycle testing, were done for burner 5, which exhibited optimal pressure drop, emissions, and flame stability behavior. For the continuous test, the burner was operated over 419 hours at an equivalence ratio of 0.6 and a mass flux rate of  $0.5 \text{ kg/m}^2\text{s}$ . The on-off cycle test was operated for 1229 cycles at the same mass flux rate as the continuous testing (Fig. 10). Thermocouples were used to measure the ambient temperature of the incoming reactants, upstream flame-arrestor section, and the interface between the flame-arrestor and downstream combustion sections. The operation cycle includes a 2-minute air purge, fuel addition to an equivalence ratio of 0.9, followed by an ignition. A standing pilot located at the top of the exhaust duct ignited the fuel-air mixture at the start of each cycle. After ignition, the temperature of the downstream element was monitored until the temperature in this section reached  $500^\circ\text{C}$ , after which the fuel flow was adjusted to an equivalence ratio of 0.6. The PMB then operates at this condition for 5 minutes, and the cycle repeats. During the continuous test over 419 hours in the combustion zone, the SiC matrix lost 1.4 grams, or 8% of total weight, from the oxidation of some of the carbon within the porous structure. Following the continuous life test, the YZA and SiC elements were undamaged, with no evidence of cracking or spalling. X-ray computed tomography (XCT) scans of the 3 ppi SiC sample before and after the durability test were used to examine the internal structural integrity of the porous matrix. A representative view of the scans is shown in Fig. 11, where it is evident that the integrity of the porous media is preserved after the extensive continuous testing. Following the cycle tests, the SiC element had lost only 0.1 grams of mass, but the XCT scans revealed a crack in the porous matrix near the interface with the upstream section. The interface region is the location of the flame during stable operation. Therefore, thermal cycling of the material resulted in fractures where fluctuations in temperature are most extreme. Coating of carbon foams with reinforcing material can potentially eliminate cracking and achieve high structural strength in PMBs. Studies using coated carbon foams have successfully achieved combustion without incurring material degradation [12, 29].

### CONCLUSION

The flame stability, pressure drop, CO and  $\text{NO}_x$  emissions, and material durability of 5 PMBs were tested and compared

to 1D volume-averaged simulation results. The results illustrate that the optimal configuration for minimizing pressure drop and maximizing flame stability is achieved using low heat conductive YZA upstream and high-conductive SiC downstream. NO<sub>x</sub> measurements were observed to increase at higher equivalence ratios and CO emissions were highest at lower flow rates, where low temperatures hinder complete CO oxidation. NO<sub>x</sub> emissions were all below 14 ppm.

Material durability testing was conducted for a burner made of 3 ppi SiC downstream section and a 40 ppi YZA upstream section. Long-term material durability tests at constant and cycled on-off conditions were done to investigate the feasibility of these materials in industrial applications. Although the 3 ppi SiC in the downstream combustion zone exhibited superior pressure drop and stability behavior, local cracks developed in the flame region during the cycle testing. Future testing should be done with reinforced material such as silicon infiltrated silicon carbide (SiSiC), which still exhibits high thermal conductivity but also has high thermal shock and corrosion resistance.

These results reinforce concepts in PMB design and optimization, and demonstrate the potential of PMBs to overcome technological barriers associated with conventional free-flame combustion technologies. To obtain more knowledge and understanding of this technology, future work concerned with detailed flow field and flame visualization needs to be done through advanced diagnostics and pore-scale simulations [7].

## ACKNOWLEDGMENT

This work is supported by a Leading Edge Aeronautics Research for NASA (LEARN) grant (Award no. NNX15AE42A).

## REFERENCES

- [1] International Civil Aviation Organization (ICAO), 2015. U.S. aviation greenhouse gas emissions reduction plan, June.
- [2] Lefebvre, A., and Ballal, D., 2010. *Gas Turbine Combustion: Alternative Fuels and Emissions*, 3rd Edition. CRC Press.
- [3] Hardesty, D. R., and Weinberg, F. J., 1973. "Burners producing large excess enthalpies". *Combustion Science and Technology*, **8**(5-6), pp. 201–214.
- [4] Kotani, Y., and Takeno, T., 1982. "An experimental study on stability and combustion characteristics of an excess enthalpy flame". In *Symposium (International) on Combustion*, Vol. 19, pp. 1503–1509.
- [5] Wood, S., and Harris, A. T., 2008. "Porous burners for lean–burn applications". *Progress in Energy and Combustion Science*, **34**(5), pp. 667–684.
- [6] Zabetakis, M. G., Lambiris, S., and Scott, G. S., 1958. "Flame temperatures of limit mixtures". *Symposium (International) on Combustion*, **7**(1), pp. 484–487.
- [7] Dunnmon, J., Sobhani, S., Wu, M., Fahrig, R., and Ihme, M., 2016. "An investigation of internal flame structure in porous media combustion via x-ray computed tomography". *Proceedings of the Combustion Institute*, **36**, pp. 4399–4408.
- [8] El-Hossaini, M. K., Maerefat, M., and Mazaheri, K., 2008. "Numerical investigation on the effects of pressure drop on thermal behavior of porous burners". *Journal of Heat Transfer*, **130**(3), p. 032601.
- [9] Malico, I., and Pereira, J. F., 2001. "Numerical study on the influence of radiative properties in porous media combustion". *Journal of Heat Transfer*, **123**(5), 03, pp. 951–957.
- [10] Noordally, E., Przybylski, J., and Witton, J., 2004. Porous media combustors for clean gas turbine engines. Tech. rep., DTIC Document.
- [11] Williams, L., and Agrawal, A. K., 2012. "Acoustic effects of porous inert media on lean premixed combustion at elevated pressures". *AIAA Paper AIAA 2012-0207*.
- [12] Vijaykant, S., and Agrawal, A. K., 2007. "Liquid fuel combustion within silicon-carbide coated carbon foam". *Experimental Thermal and Fluid Science*, **32**(1), pp. 117–125.
- [13] Bedoya, C., Dinkov, I., Habisreuther, P., Zarzalis, N., Bockhorn, H., and Parthasarathy, P., 2015. "Experimental study, 1d volume-averaged calculations and 3d direct pore level simulations of the flame stabilization in porous inert media at elevated pressure". *Combustion and Flame*, **162**(10), pp. 3740–3754.
- [14] Bakry, A., Al-Salaymeh, A., Al-Muhtaseb, A. H., Abu-Jrai, A., and Trimis, D., 2011. "Adiabatic premixed combustion in a gaseous fuel porous inert media under high pressure and temperature: Novel flame stabilization technique". *Fuel*, **90**(2), pp. 647–658.
- [15] Babkin, V. S., Korzhavin, A. A., and Bunev, V. A., 1991. "Propagation of premixed gaseous explosion flames in porous media". *Combustion and Flame*, **87**, pp. 182–190.
- [16] Barra, A. J., Diepvans, G., Ellzey, J. L., and Henneke, M. R., 2003. "Numerical study of the effects of material properties on flame stabilization in a porous burner". *Combustion and Flame*, **134**(4), pp. 369–379.
- [17] Philipse, A. P., and Schram, H. L., 1991. "Nondarcian airflow through ceramic foams". *Journal of the American Ceramic Society*, **74**(4), 4, pp. 728–732.
- [18] Ergun, S., and Orning, A. A., 1949. "Fluid flow through randomly packed columns and fluidized beds". *Industrial & Engineering Chemistry*, **41**(6), pp. 1179–1184.
- [19] Wawrzinek, K., and Trimis, D., 2004. "Flame stabilization of highly diffusive gas mixtures in porous inert media". In *Modelling Fluid Flow: The State of the Art*, J. Vad, T. Lajos, and R. Schilling, eds., Springer, pp. 107–121.
- [20] Kaviany, M., 2012. *Principles of Heat Transfer in Porous*

- Media*. Springer New York.
- [21] Vafai, K., ed., 2005. *Handbook of Porous Media*. CRC Press.
  - [22] Hirschfelder, J. O., and Curtiss, C. F., 1949. “Theory of propagation of flames. Part I: General equations”. *Symposium on Combustion and Flame, and Explosion Phenomena*, **3**(1), pp. 121–127.
  - [23] Fu, X., Viskanta, R., and Gore, J. P., 1998. “Measurement and correlation of volumetric heat transfer coefficients of cellular ceramics”. *Experimental Thermal and Fluid Science*, **17**(4), pp. 285–293.
  - [24] Howell, J., Menguc, M., and Siegel, R., 2010. *Thermal Radiation Heat Transfer, 5th Edition*. Taylor & Francis.
  - [25] Hsu, P.-F., and Howell, J. R., 1992. “Measurements of thermal conductivity and optical properties of porous partially stabilized zirconia”. *Experimental Heat Transfer*, **5**(4), pp. 293–313.
  - [26] Goodwin, D. G., 1998. CANtera: An open-source, object-oriented software suite for combustion.
  - [27] Innocentini, M. D., Salvini, V. A. R., Macedo, A., and Pandolfelli, V. C., 1999. “Prediction of ceramic foams permeability using Ergun’s equation”. *Materials Research*, **2**, pp. 283–289.
  - [28] Dukhan, N., and Patel, P., 2008. “Equivalent particle diameter and length scale for pressure drop in porous metals”. *Experimental Thermal and Fluid Science*, **32**(5), pp. 1059–1067.
  - [29] Marbach, T. L., and Agrawal, A. K., 2003. “Experimental study of surface and interior combustion using composite porous inert media”. In ASME Turbo Expo 2003, collocated with the 2003 International Joint Power Generation Conference, American Society of Mechanical Engineers, pp. 549–556.